IIETA International Information and Engineering Technology Association
Advancing the World of Information and Engineering

Mathematical Modelling of Engineering Problems
Vol. 12, No. 10, October, 2025, pp. 3510-3518
Journal homepage: http://iieta.org/journals/mmep

A Numerical Study on the Effect of Layer Thickness of Phase Change Material and Metal Foam in a Photovoltaic Thermal System

Bernardo Buonomo*, Maria Rita Golia, Oronzio Manca, Sergio Nardini

Dipartimento di Ingegneria, Università degli Studi della Campania "Luigi Vanvitelli", Aversa 81031, Italy

Corresponding Author Email: bernardo.buonomo@unicampania.it

https://doi.org/10.18280/mmep.121017

Received: 12 August 2025
Revised: 13 October 2025
Accepted: 25 October 2025
Available online: 31 October 2025

Keywords:
PCM, metal foam, solar energy, photovoltaic

ABSTRACT

Photovoltaic (PV) modules typically convert only 5–25% of incident solar radiation into electricity, with the remainder generating heat that often goes unused. A promising solution is the integration of hybrid photovoltaic thermal (PVT) systems, which simultaneously produce electricity and recover thermal energy. This study numerically investigates a PVT module enhanced with phase change material (PCM) and metal foam (MF) layers of varying thicknesses, under both summer and winter conditions. The analysis evaluates the impact of combined PCM-MF layer thickness on thermal storage and overall system performance. The heat transfer fluid (water) is simulated to circulate only during daylight hours when beneficial, based on the outlet-inlet temperature difference. Simulations are performed using Fluent Computational Fluid Dynamics (CFD) software for a system located in Aversa, Italy, at an optimal tilt angle of 30°, with RT21 paraffin as the PCM. Results are reported in terms of PV panel temperatures, operational duration, and thermal and electrical energy outputs, with the aim of validating the simulation model's accuracy in representing real-world thermal behavior.

1. INTRODUCTION

Photovoltaic (PV) modules currently convert only 5% to 25% of the incoming solar radiation into electricity, with the majority of the energy being dissipated as heat within the module, often going unused. Hybrid photovoltaic thermal (PVT) systems, on the other hand, are designed to capture this excess thermal energy and convert it into usable heat, while still generating electricity through the PV cells [1]. Mousavi et al. [2] demonstrated that the incorporation of phase change materials (PCMs) and metal foams (MFs) into PVT panels can significantly enhance both electrical and exergy efficiency. Their findings indicated that configurations lacking an optimized combination of PCM and MF exhibited noticeably lower thermal performance. In the specific climatic conditions of Benha, Egypt, Sharaf et al. [3] analyzed the annual energy and exergy output of a PV panel enhanced with aluminum metal foam embedded in pure PCM. Their results showed that coupling PCM with PV panels led to improved energy conversion efficiency and higher electricity generation. They emphasized the importance of selecting appropriate PCMs to maximize system performance. Dayer et al. [4] explored a three-dimensional model of a PV/T system that integrates copper metal foam and PCM. Their design helped lower the surface temperature of the PV panel, thus boosting electrical efficiency. Under test conditions of 1000 W/m² solar irradiance and 20°C ambient temperature, the system reached thermal and electrical efficiencies of 65% and 13%, respectively. Sharaf et al. [5] further confirmed the effectiveness of PCMs in absorbing surplus heat from PV panels. During periods of high solar intensity, the latent heat stored in the PCM helped maintain PV panel temperatures below 25°C, leading to enhanced thermal and electrical performance of the hybrid system. Alsaqoor et al. [6] studied the influence of PCM integration on PVT systems and developed a graphical interface in MATLAB Simulink using climate data from Amman, Jordan. Their analysis revealed that the inclusion of PCM increased the peak electrical output from 18 kW (without PCM) to 21 kW (with PCM). According to Bandaru et al. [7] systems that combine PVT with PCM can store up to 50% more thermal energy than conventional water-based PVT setups. This not only improves electrical output but also prolongs the availability of usable thermal energy. However, improper PCM selection may cause issues such as low thermal conductivity and suboptimal charging/discharging behavior, necessitating further experimentation to ensure long-term system reliability and prevent leakage. Hossain et al. [8] applied PCM in the design of a hybrid solar PVT unit and assessed its performance against climate data from Malaysia. The study revealed that PCMs positively impacted both the electrical and thermal efficiency of PV panels. Maximum efficiencies for PVT and PVT-PCM systems were recorded at 14.57% and 15.32% (electrical), and 75.29% and 86.19% (thermal), respectively. Noxpanco et al. [9] underscored the importance of conducting a cost-benefit analysis of PV/T systems. They highlighted the challenge of acquiring precise pricing data and advocated for more readily accessible economic information to support

informed engineering and design decisions. Additionally, they recommended enhancing the aesthetic appeal of PV/T systems to boost user acceptance and deployment. Dayer et al. [10] conducted an experimental and numerical study on a PVT collector enhanced with a PCM and a copper foam matrix, achieving thermal efficiencies of up to 72.74% and a peak electrical efficiency of 10.74%. The design incorporates serpentine tubes and exploits the synergy between PCM and Copper foam to ensure effective thermal management and improved overall system performance under real-world conditions. Alipour et al. [11] examined the effect of metal foam porosity in a PVT system integrated with PCM, using nanofluids as the cooling medium. Parametric analysis reveals that increasing foam porosity from 0.2 to 0.8 leads to a 33% improvement in thermal efficiency, with only a slight drop in electrical efficiency. Adding copper foam boosts thermal efficiency by 25.4% compared to standard PVT/PCM configurations. Chang et al. [12] investigated the thermal and electrical performance of a PVT system with a receiver tube filled with a PCM-copper foam composite. Results show a 37.33% increase in thermal efficiency and a 0.2% rise in electrical efficiency. The integration of porous copper foam significantly enhances heat transfer, with seasonal performance optimized via Computational Fluid Dynamics (CFD) simulations. Lastly, Elavarasan et al. [13] offered a comprehensive review of passive cooling technologies for PV modules using PCM. The authors propose a conceptual framework for selecting the most suitable PCM based on thermophysical properties, container designs, and environmental conditions. Hybrid techniques to enhance thermal conductivity, such as the integration of metal foams and extended surfaces, are also discussed.

The purpose of this article is to develop a 2D PVT module consisting of a heat transfer channel positioned above a layer of PCM combined with metal foam. This configuration aims to provide the panel with thermal energy storage capabilities, allowing it to operate for a longer duration compared to a conventional PVT panel. The 2D simulations were conducted in Aversa, Italy, with the panel tilted at 30° and oriented southward. ANSYS Fluent was used as the simulation tool. A typical day was analyzed for the months of January, June, July, and December to capture seasonal variations. For the simulations, RT21 was selected as the PCM, with a melting point between 21°C and 23°C, in combination with aluminum metal foam and a heat transfer fluid temperature of 293.15 K. From previous studies by Buonomo et al. [14], it emerged that RT21, compared to RT25, allowed for the creation of a more efficient photovoltaic thermal panel. In fact, the selected photovoltaic panel showed optimal performance at 21°C. The results are presented in terms of panel temperature, PCM liquid fraction, and panel efficiency throughout the course of the day and power output.

2. MODULE DESCRIPTION

The analysis was conducted on a PVT panel module configured as illustrated in Figure 1.

The module is assumed to be fully enclosed. The layer referred to as the "PV layer" comprises the assembly of the glass cover, photovoltaic cell, EVA (Ethylene Vinyl Acetate), adhesive material, and Tedlar. The material properties and relevant data for these components are provided in Table 1. The PV layer was schematized by considering equivalent thermal conductivity and average specific heat capacity and density, the values are listed in Table 2.

The configuration in Figure 1 includes a thermal storage layer composed of RT21 as PCM mixed with metal foam (MF), positioned beneath the heat transfer fluid channel. The thermal properties of RT21 are listed in Table 3. This configuration was examined using three different thicknesses of the storage layer: 0.5 cm, 1.0 cm, and 2.0 cm. The purpose of this setup is to evaluate the influence of the storage layer's thickness on both thermal and electrical power generation during a representative day in the months of January, June, July, and December.

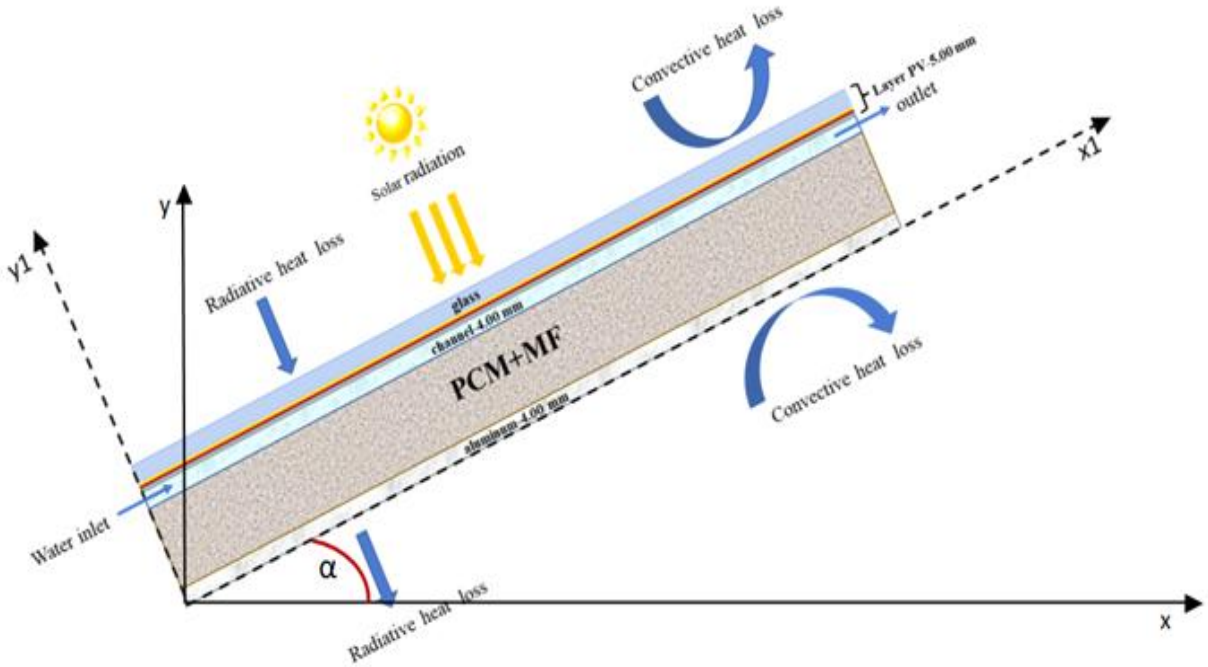

Figure 1. Cross-sectional view of the analyzed PVT module with the integrated PCM+MF layer

Table 1. Properties of components

Glass		PV	
α	0.01	α	0.93
ρ [kg·m^{-3}]	2700	ρ [kg·m^{-3}]	2328
γ	0.16	ε	0.90
ε	0.90	ηref	0.126
C [J·kg^{-1}·K^{-1}]	800	Tref [K]	294
λ [W·m^{-1}·K^{-1}]	1.80	C [J·kg^{-1}·K^{-1}]	677
s [mm]	4	λ [W·m^{-1}·K^{-1}]	140
τ	0.95	β [K^{-1}]	0.0052
EVA		s [mm]	0.35
λ [W·m^{-1}·K^{-1}]	0.2	τ	0.01
s [mm]	0.1	TEDLAR	
ADHESIVE		λ [W·m^{-1}·K^{-1}]	0.35
λ [W·m^{-1}·K^{-1}]	0.85	s [mm]	0.5
s [mm]	0.05		

Table 2. Proprieties of PV-layer

PV-Layer		
Average Specific Heat Capacity	**Average Density**	**Equivalent Thermal Conductivity**
738.5 J kg^{-1}·K^{-1}	2514 kg·m^{-3}	1.18 W m^{-1}·K^{-1}

Table 3. Properties of RT21 [15]

Property	Value
ρ [kg·m^{-3}]	825
H_L [kJ·kg^{-1}]	190
C [J·kg^{-1}·K^{-1}]	2000
λ [W·m^{-1}·K^{-1}]	0.2
T_s [K]	294.15
T_l [K]	296.15

3. ENERGY EQUATIONS AND BOUNDARY CONDITIONS

In this investigation, the following assumptions were adopted:

- The materials composing each layer of the PV panel are treated as homogeneous and isotropic.
- Incident solar radiation on the front side of the PV module is assumed to be uniformly distributed.
- Electrical contact resistances within the PV cell are disregarded in this study.
- The phase transition of the PCM is considered to occur through both conductive and convective heat transfer mechanisms.
- The influence of rainfall, which could potentially alter the rate of dust deposition, is excluded from the analysis.
- The system is modeled using governing equations expressed in terms of pressure and velocity fields.
- The thermal behavior of the PCM is simulated using the enthalpy-porosity technique as developed by Voller and Prakash.
- The flow characteristics of the heat transfer fluid (HTF), specifically water, within the channel are modeled as unsteady, incompressible, laminar, and two-dimensional.
- The natural convection of molten PCM inside its container is also treated as unsteady, laminar, incompressible, and two-dimensional.
- The porous domain is considered to be saturated with fluid and to possess a uniform and isotropic structure.
- The flow through the porous region is described using the extended Darcy model that includes Brinkman and Forchheimer terms.
- Except for density, which is assumed to vary linearly with temperature according to the Boussinesq approximation, all other thermo-physical properties are considered constant and evaluated at the ambient temperature.
- Heat transfer within the porous medium is analyzed under the assumption of local thermal equilibrium (LTE) between solid and fluid phases.

3.1 Energy equation for PV-layer

The energy equation for PV-layer is:

$$(\rho C)_{PV-layer}\frac{\partial T}{\partial \tau}=\lambda_{PV-layer}\left(\frac{\partial^2 T}{\partial x^2}+\frac{\partial^2 T}{\partial y^2}\right)+Q \qquad (1)$$

where, ρ is the density, C is the heat capacity (J/(kg·K)) and λ is the thermal conductivity and Q is the internal heat source.

It is assumed that the fraction of solar radiation absorbed by the PV panel but not converted into electrical energy is entirely transformed into thermal energy. This thermal energy acts as an internal heat source, leading to a rise in the panel's temperature. The rate of heat generation, denoted as Q is quantified using the corresponding governing Eq. (2):

$$Q=\frac{(1-\eta_{el})G_i A}{V_{PV}} \qquad (2)$$

where, G_i is the absorbed solar radiation, A is the upper surface of the PV panel and V_{pv}, cell is the volume of the PV cells in the panel.

3.2 Aluminium layer

The energy equation of the aluminium layer is:

$$(\rho C)_{al}\frac{\partial T}{\partial \tau}=\lambda_{al}\left(\frac{\partial^2 T}{\partial x^2}+\frac{\partial^2 T}{\partial y^2}\right) \qquad (3)$$

where, ρ is the density, C is the heat capacity (J/(kg·K)) and λ is the thermal conductivity.

3.3 Channel layer

The equation that governs the motion for the channel is:

$$\rho\left(\frac{\partial u}{\partial \tau}+u\frac{\partial u}{\partial x}+v\frac{\partial u}{\partial y}\right)=-\frac{\partial p}{\partial x}+\mu\left(\frac{\partial^2 u}{\partial x^2}+\frac{\partial^2 u}{\partial y^2}\right) \qquad (4)$$

$$\rho\left(\frac{\partial v}{\partial \tau}+u\frac{\partial v}{\partial x}+v\frac{\partial v}{\partial y}\right)=-\frac{\partial p}{\partial y}+\mu\left(\frac{\partial^2 v}{\partial x^2}+\frac{\partial^2 v}{\partial y^2}\right) \qquad (5)$$

where, P is the pressure, v is the velocity vector, μ is the dynamic viscosity and ρ is the density.
The energy equation is:

$$(\rho C)_f \left[\frac{\partial T}{\partial t} + \left(u \frac{\partial T}{\partial x} + v \frac{\partial T}{\partial y} \right) \right] = \lambda_f \left(\frac{\partial^2 T}{\partial x^2} + \frac{\partial^2 T}{\partial y^2} \right) \quad (6)$$

3.4 PCM and metal foam layer

Continuity equation, momentum and energy equations in LTE, were used for PCM and MF.

Continuity equation:

$$\frac{\partial u}{\partial x} + \frac{\partial u}{\partial y} = 0 \quad (7)$$

Momentum equations:

(momentum x)

$$\frac{\rho_{pcm}}{\varepsilon_P}\left(\frac{\partial u}{\partial \tau} + \frac{u}{\varepsilon_P}\frac{\partial u}{\partial x} + \frac{v}{\varepsilon_P}\frac{\partial u}{\partial y} \right) = -\frac{\partial p}{\partial x} + \frac{\mu_{pcm}}{\varepsilon_P}\left(\frac{\partial^2 u}{\partial x^2} + \frac{\partial^2 u}{\partial y^2} \right) - \frac{(1-\beta_l)^2}{(\beta_l^3 - 0.001)^3} A_{mush} u + -\left(\frac{\mu_{pcm}}{K} + \frac{C_F \rho_{pcm}}{\sqrt{K}} |V| \right) u + \rho_{pcm} \gamma (T - T_{melt}) g \cos(\alpha) \quad (8)$$

(momentum y)

$$\frac{\rho_{pcm}}{\varepsilon_P}\left(\frac{\partial v}{\partial \tau} + \frac{u}{\varepsilon_P}\frac{\partial v}{\partial x} + \frac{v}{\varepsilon_P}\frac{\partial v}{\partial y} \right) = -\frac{\partial p}{\partial y} + \frac{\mu_{pcm}}{\varepsilon_P}\left(\frac{\partial^2 v}{\partial x^2} + \frac{\partial^2 v}{\partial y^2} \right) - \frac{(1-\beta_l)^2}{(\beta_l^3 - 0.001)^3} A_{mush} v + -\left(\frac{\mu_{pcm}}{K} + \frac{C_F \rho_{pcm}}{\sqrt{K}} |V| \right) v + \rho_{pcm} \gamma (T - T_{melt}) g \sin(\alpha) \quad (9)$$

Energy equation in LTE:

$$(\rho C)_{eff} \frac{\partial v}{\partial \tau} + (\rho C)_{pcm} \left(u \frac{\partial T}{\partial x} + v \frac{\partial T}{\partial y} \right) = \lambda_{eff} \left(\frac{\partial^2 T}{\partial x^2} + \frac{\partial^2 T}{\partial y^2} \right) - \varepsilon_P \rho_{pcm} H_L \frac{\partial \beta}{\partial \tau} \quad (10)$$

In Eq. (10), H_L represents the latent heat of the PCM, and t is the time.

$$(\rho C)_{eff} = (1-\varepsilon_P)\rho_{mf} C_{mf} + \varepsilon_P \rho_p C_{pcm} \quad (11)$$

$$\lambda_{eff} = (1-\varepsilon_P)\lambda_{mf} + \varepsilon_P \lambda_{pcm} \quad (12)$$

Eq. (10) is a weighted average value and Eq. (11) is the effective thermal conductivity. ρ_{mf}, ρ_{pcm} and c_{mf}, c_{pcm} represent the density and specific heat of MF and PCM (pcm). λ_{mf} and λ_{pcm} are the metal foam and PCM thermal conductivities.

4. PERFORMANCE EVALUATION

The performance evaluation of the PVT module was carried out using the following set of equations. The pointwise electrical efficiency, η_{el}, of the PV cells is defined according to the formulation provided by Nouira and Sammouda [16]:

$$\eta_{el} = \eta_{ref}(1 - \beta_{ref}(T_{PV} - T_{ref})) \quad (13)$$

In this expression, the parameters η_{ref}, β_{ref} and T_{ref}, and refers to specific panel characteristics, which are detailed in Table 1. The instantaneous electrical power output of the module is computed using the following relation:

$$P_{out} = \eta_{el} A G_i \quad (14)$$

To estimate the annual energy production, the average value of the obtained power is multiplied by the total number of operating hours over a full year. Data for ambient temperature and solar radiation were sourced from the PVGIS database. The variation in sky temperature, T_{sky}, was estimated using the empirical correlation proposed by Swinbank [17]:

$$T_{sky} = 0.0552 \cdot T_{amb}^{\ 1.5} \quad (15)$$

Both the thermal energy extracted by the circulating water and the thermal energy attributed to the PCM were evaluated. For the fluid flow through the channel, the heat transfer rate is given by:

$$\dot{E}_f = \dot{m}_f C_f (T_{f,out} - T_{f,in}) \quad (16)$$

here, $\dot{m}_f$ denotes the mass flow rate, C_f is the specific heat capacity of the fluid and $T_{f,out}$, $T_{f,in}$ are the inlet and outlet temperatures of the heat transfer fluid. In this analysis, the inlet temperature is maintained constant, assuming active thermal regulation within the system. Integration of this rate over time yields the total thermal energy delivered by the channel:

$$W_f = \int E_f(t) dt \quad (17)$$

A similar procedure was followed for quantifying the thermal energy contribution of the PCM. Starting from the enthalpy formulation of the PCM, its time derivative provides the rate of heat release or absorption:

$$\dot{E}_{PCM} = \frac{dH}{dt} \quad (18)$$

Temporal integration of this expression gives the total amount of thermal energy stored or released by the PCM:

$$W_{PCM} = \int E_{PCM}(t) dt \quad (19)$$

In Eq. (21), the numerator represents the thermal power extracted by the channel, while G_i corresponds to the solar irradiance incident on the surface of the PVT system [18].

$$\dot{E}_{sun} = \tau_g \alpha_{PV} G_i A_{PV} \tag{20}$$

Regarding thermal performance, a comparison between the PVT system with and without PCM reveals that the configuration without PCM yields higher thermal efficiency, as observed in Preet et al. [19]. The thermal efficiency of the heat transfer fluid alone, excluding any contributions from the PCM, is given by Duffie and Beckman [20]:

$$\eta_{th,f} = \frac{\dot{E}_f}{\dot{E}_{sun}} \tag{21}$$

In the present configuration, no heat transfer tube is embedded within the PCM layer. Instead, a novel layout of the PVT system is considered, wherein the PCM layer acts as a thermal resistance. Consequently, the thermal energy output from the panel is determined by:

$$\dot{E}_{th} = \dot{E}_f \tag{22}$$

For model validation, reference was made to the study by Park et al. [21], in which a photovoltaic panel measuring 350 mm × 280 mm was simulated both with and without a 30 mm thick PCM layer. The validation approach adopted in the present work follows the same methodology employed by Buonomo et al. [14].

5. RESULTS

5.1 Liquid fraction, PV temperature and outlet temperature

The temperatures of both PV layer and the PCM, as well as the liquid fraction of the PCM, were analyzed for varying storage layer thicknesses of s = 0.5 cm, 1.0 cm, and 2.0 cm. The simulations were conducted under a constant HTF inlet temperature of 293.15 K, for representative days in January, June, July, and December- two typical days from the winter season and two from the summer.

The results show that during the winter months, PCM does not undergo phase transition regardless of its thickness. This behavior is attributed to the positioning of the PCM layer beneath the HTF channel, coupled with the insufficient thermal energy input during these periods. The ambient temperatures remain relatively low, and the limited solar radiation is not enough to heat both the HTF and the PCM simultaneously to the melting point of the storage material.

This trend is further confirmed by observing the PV panel temperature in December (see Figure 2), where no significant variation is detected with respect to changes in PCM thickness. The thermal response of the PV layer remains nearly unchanged, indicating that the PCM layer does not influence the thermal dynamics of the system in cold conditions due to the lack of melting. In the month of July, Figure 3, however, the temperature of the photovoltaic panel varies depending on the thickness of the PCM; it is lower when the PCM thickness is greater.

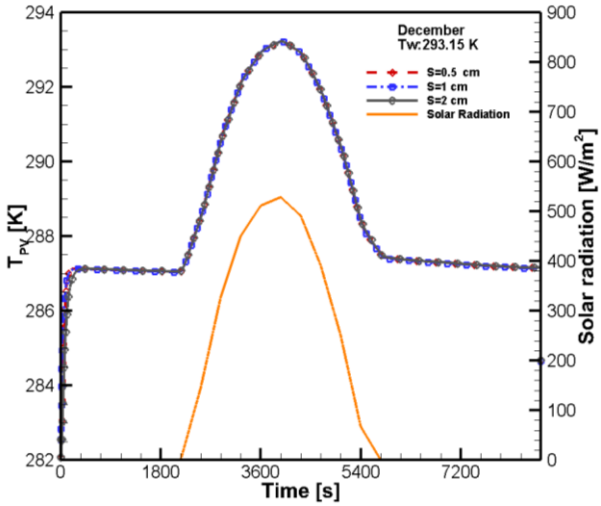

Figure 2. Temporal evolution of PV temperature during a typical December day for s = 0.5 cm, 1.0 cm, and 2.0 cm

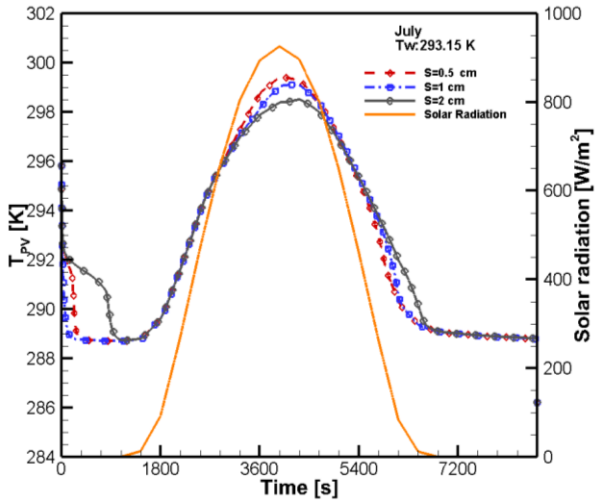

Figure 3. Temporal evolution of PV temperature during a typical July day for s = 0.5 cm, 1.0 cm, and 2.0 cm

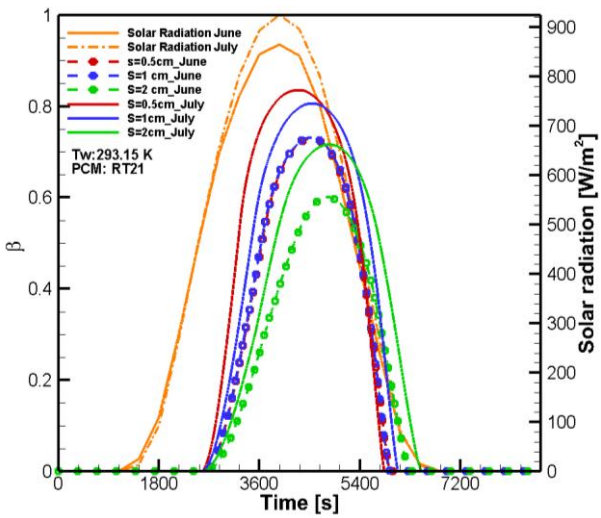

Figure 4. Temporal evolution of the liquid fraction during a typical day in June and July for different thicknesses of the PCM+MF layer

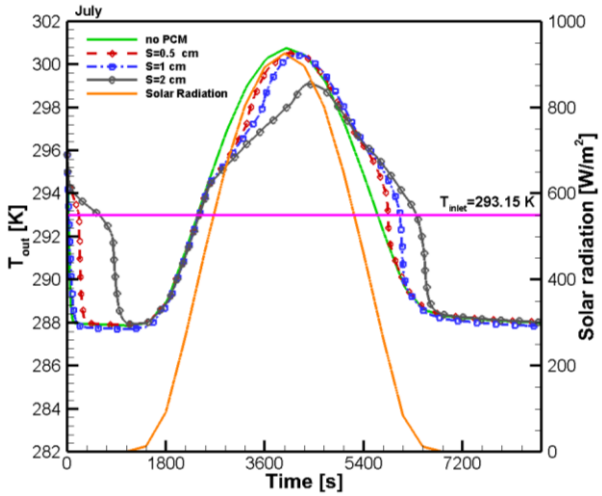

Figure 5. Comparison of the temporal evolution of outlet heat transfer fluid temperature for the case without PCM and with s = 0.5 cm, 1.0 cm, and 2.0 cm in July

In Figure 4, the liquid fraction is shown for typical days in July and June. As expected, greater thickness corresponds to lower liquid fractions. Furthermore, the PCM reaches a higher liquid fraction during the month of July. The position of the layer beneath the heat transfer channel does not allow for complete melting of the PCM.

By analyzing the outlet temperature of the HTF, Figure 5, as the PCM thickness varies, it can be observed that greater PCM thicknesses correspond to lower HTF outlet temperatures. This indicates that the PCM absorbs excess heat from the HTF and, consequently, from the PV panel. In cases with PCM thicknesses of 0.5 cm and 1 cm, the reduction in outlet temperature is minimal. However, with a thickness of 2.0 cm, a decrease of approximately 2°C is observed at the peak on solar radiation. Additionally, the outlet temperature curve is shifted to the right, indicating that once the PCM begins to melt, it starts contributing to the thermal regulation of the water in the channel.

5.2 Electrical energy

The average day of January, June, July, and December was used for the simulations, and the results were presented in terms of power output, electrical efficiency, and operating hours of the PV panel.

Only the hours with solar irradiation—corresponding to the actual working hours of the PV panel—were considered from the electrical performance perspective of the module.

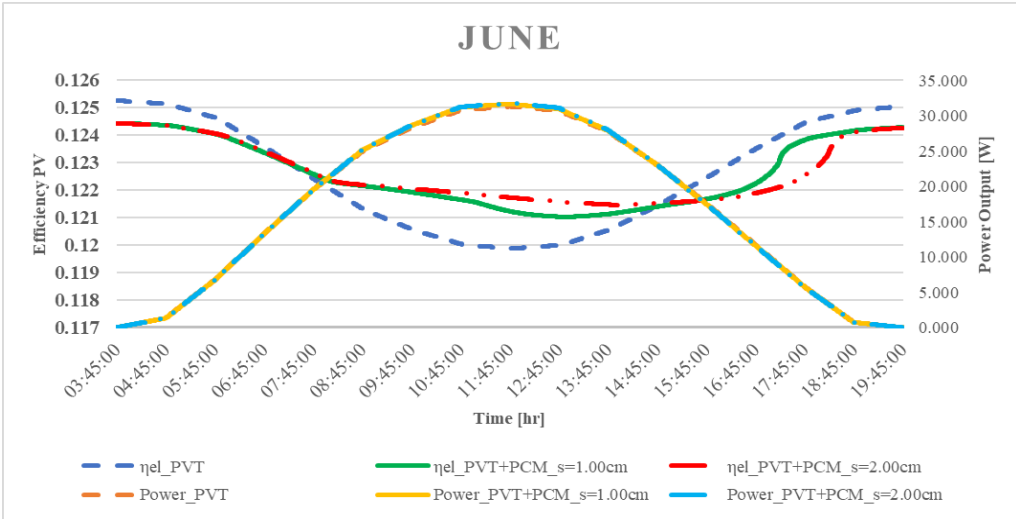

(a) Typical day of June

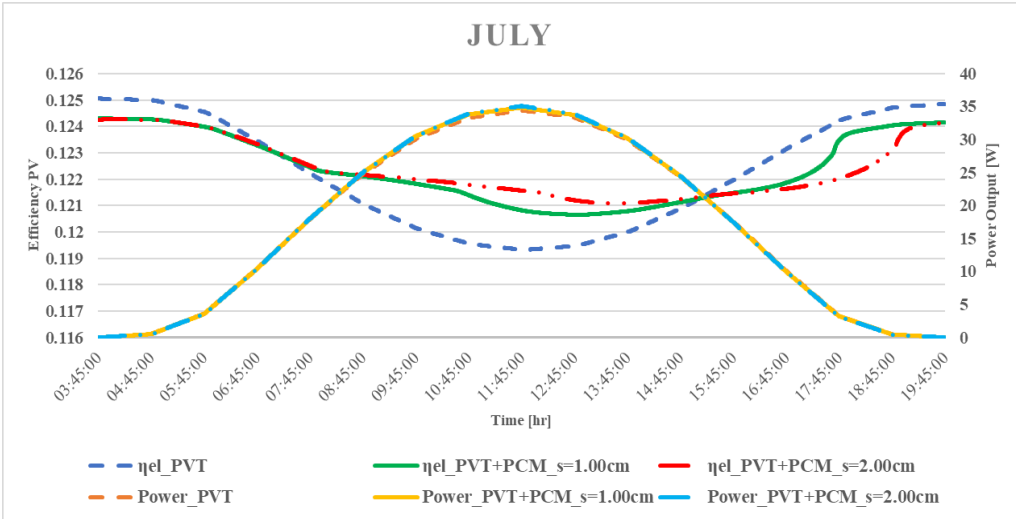

(b) Typical day of July

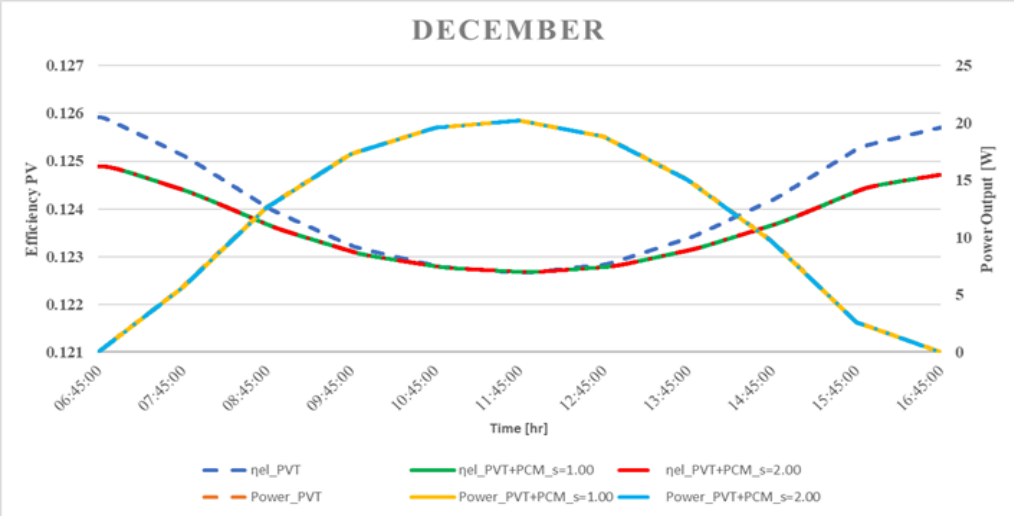

(c) Typical day of December

Figure 6. Time evolution of efficiency and power output

Table 4. Operating hours

Month	No. PCM	PCM + MF, s = 1.00 cm	Percentage Increase (%)	PCM + MF, s = 2.00 cm	Percentage Increase (%)
June	8.4 h	9.5 h	13.1%	10.1 h	21.4%
July	9 h	10.1 h	12.2%	12.2 h	35.5%

The graphs in Figure 6 show that the PV module with the PCM+MF layer exhibits higher electrical efficiency compared to the module without the thermal storage layer. However, during the winter months, it was observed that, due to the position of the PCM and MF layer and its inability to fully melt, the electrical efficiency of the panel with and without PCM is nearly the same.

Furthermore, although the electrical efficiency of the panel during the summer months is higher in the presence of the PCM+MF layer, the increase is not sufficient to result in a significant improvement in overall electricity production, as illustrated in Figure 6.

5.3 Thermal energy

Although the system does not exhibit significant improvements in thermal energy efficiency, it does demonstrate an extended operating period. This effect is noticeable on the selected days during the summer months, but not during the winter months. This is primarily due to the inability of the PCM to melt in December and January, regardless of its thickness. The percentage increase when using a panel with a PCM+MF layer is approximately 13.1% and 21.4% for layer thicknesses of 1 cm and 2 cm, respectively, in the month of June, and about 12.2% and 35.5% for the same thicknesses in July. Cold months do not show any thermal performance improvements. Therefore, it can be concluded that the presence of the PCM+MF layer primarily contributes to an extension of the module's operating hours. These operating hours were calculated based on the condition that the outlet temperature is higher than the inlet temperature as shown in Table 4.

6. CONCLUSIONS

The integration of a PCM+MF layer into the PVT system demonstrates potential benefits primarily in terms of thermal regulation and extended operational time, rather than marked improvements in thermal or electrical efficiency. During summer months, the presence of the PCM layer contributes to a reduction in PV panel temperature and leads to a moderate percentage increase in operating hours—up to 35.5% with a 2 cm layer in July. However, the thermal and electrical enhancements remain limited, with no significant impact on overall electricity generation. In winter months, PCM does not undergo phase transition due to insufficient solar energy and its position beneath the HTF channel, resulting in negligible influence on both the thermal and electrical behavior of the system.

Therefore, while the use of PCM+MF can enhance thermal management and slightly prolong operational periods during high-irradiance conditions, its effectiveness is season-dependent and limited under low-radiation scenarios.

It is thus necessary to reconsider the current PVT module configuration and explore alternative placements or designs for the PCM+MF layer. Although the potential benefits of thermal storage and temperature regulation are evident, in the configuration studied, PCM behaves more as a thermal resistance than as an effective thermal storage medium or temperature regulator for the PV panel.

ACKNOWLEDGMENT

This work was supported by the Italian Government PNRR Grant No. PE00000021 – PNRR - Mission 4 - Component 2 - Investment 1.3 – Funded by the European Union – NextGenerationEU - Ministerial Decree No. 341 dated 15.03.2022 – Cascade Call for the Extended Partnership “NEST - Network 4 Energy Sustainable Transition” Spoke 7 "Smart Sector Integration" – Ministerial Decree No. 800 dated on 24 June, 2024.

REFERENCES

[1] Preet, S. (2021). A review on the outlook of thermal management of photovoltaic panel using phase change material. Energy and Climate Change, 2: 100033. https://doi.org/10.1016/j.egycc.2021.100033

[2] Mousavi, S., Kasaeian, A., Shafii, M.B., Jahangir, M.H. (2018). Numerical investigation of the effects of a copper foam filled with phase change materials in a water-cooled photovoltaic/thermal system. EEnergy Conversion and Management, 163: 187-195. https://doi.org/10.1016/j.enconman.2018.02.039

[3] Sharaf, M., Yousef, M.S., Huzayyin, A.S. (2022). Year-round energy and exergy performance investigation of a photovoltaic panel coupled with metal foam/phase change material composite. Renewable Energy, 189: 777-789. https://doi.org/10.1016/j.renene.2022.03.071

[4] Dayer, M., Sopian, K., Ibrahim, A., Al-Aasam, A.B., Abdulsahib M., B., Rahmanian, S., Abd Hamid, A.S. (2023). Performance of combined PCM/metal foam-based photovoltaic thermal (PVT) collector. International Journal of Renewable Energy Research, 13(2). https://doi.org/10.20508/ijrer.v13i2.13881.g8723

[5] Sharaf, M., Yousef, M.S., Huzayyin, A.S. (2022). Review of cooling techniques used to enhance the efficiency of photovoltaic power systems. Environmental Science and Pollution Research, 29: 26131-26159. https://doi.org/10.1007/s11356-022-18719-9

[6] Alsaqoor, S., Alqatamin, A., Alahmer, A., Nan, Z., Al-Husban, Y., Jouhara, H. (2023). The impact of phase change material on photovoltaic thermal (PVT) systems: A numerical study. International Journal of Thermofluids, 18: 100365. https://doi.org/10.1016/j.ijft.2023.100365

[7] Bandaru, S.H., Becerra, V., Khanna, S., Radulovic, J., Hutchinson, D., Khusainov, R. (2021). A review of photovoltaic thermal (PVT) technology for residential applications: Performance indicators, progress, and opportunities. Energies, 14(13): 3853. https://doi.org/10.3390/en14133853

[8] Hossain, M.S., Kumar, L., Arshad, A., Selvaraj, J., Pandey, A.K., Rahim, N.A. (2023). A comparative investigation on solar PVT- and PVT-PCM-based collector constancy performance. Energies, 16(5): 2224. https://doi.org/10.3390/en16052224

[9] Noxpanco, M.G., Wilkins, J., Riffat, S. (2020). A review of the recent development of photovoltaic/thermal (PV/T) systems and their applications. Future Cities and Environment, 6(1). https://doi.org/10.5334/fce.97

[10] Dayer, M., Shahid, M.A., Sopian, K., Kazem, H.A., Al-Aasam, A.B., Abdulsahib, B., Al-Waeli, A.H.A. (2024). Experimental and numerical assessments of a photovoltaic thermal collector equipped with newly configured cooling methods using PCM/CFM. Solar Energy, 276: 112659. https://doi.org/10.1016/j.solener.2024.112659

[11] Alipour, N., Jafari, B., Hosseinzadeh, K. (2024). Analysis of the impact of metal foam with phase change material on solar photovoltaic thermal system efficiency. Journal of Energy Storage, 98: 113064. https://doi.org/10.1016/j.est.2024.113064

[12] Chang, S.B., Liu, H.T., Li, G. (2025). Effect of installing porous metal insertion inside the collector tube of a photovoltaic thermal system integrated with PCM-copper foam composite. Energy, 314: 134203. https://doi.org/10.1016/j.energy.2024.134203

[13] Elavarasan, M.R., Pugazhendhi, R., Shafiq, S., Gangatharan, S., Nadarajah, M., Shafiullah, G.M. (2025). Efficiency enhancement of PV panels with passive thermal management using PCM: An exhaustive review on materials, designs and effective techniques. Applied Energy, 382: 125217. https://doi.org/10.1016/j.apenergy.2024.125217

[14] Buonomo, B., Golia, M.R., Manca, O., Nardini, S., Plomitallo, R.E. (2024). 2D simulation of photovoltaic thermal panel module with a layer of phase change material and metal foam. In Proceedings of the 9th CHT-24 ICHMT International Symposium on Advances in Computational Heat Transfer, Begellhouse, Connecticut, USA, pp. 429-447. https://doi.org/10.1615/ICHMT.2024.CHT-24.390

[15] Rubitherm Technologies GmbH. PCM RT-LINE Versatile Organic PCM for Your Application. https://www.rubitherm.eu/en/productcategory/organische-pcm-rt.

[16] Nouira, M., Sammouda, H. (2018). Numerical study of an inclined photovoltaic system coupled with phase change material under various operating conditions. Applied Thermal Engineering, 141: 958-975. https://doi.org/10.1016/j.applthermaleng.2018.06.039

[17] Swinbank, W.C. (1963). Long-wave radiation from clear skies. Quarterly Journal of the Royal Meteorological Society, 89(381): 339-348. https://doi.org/10.1002/qj.49708938105

[18] Abbas, S., Zhou, J., Hassan, A., Yuan, Y., Yousuf, S., Sun, Y., Zeng, C. (2023). Economic evaluation and annual performance analysis of a novel series-coupled PV/T and solar TC with solar direct expansion heat pump system: An experimental and numerical study. Renewable Energy, 204: 400-420. https://doi.org/10.1016/j.renene.2023.01.032

[19] Preet, S., Bhushan, B., Mahajan, T. (2017). Experimental investigation of water based photovoltaic/thermal (PV/T) system with and without phase change material (PCM). Solar Energy, 155: 1104-1120. https://doi.org/10.1016/j.solener.2017.07.040

[20] Duffie, J.A., Beckman, W.A. (2013). Solar Engineering of Thermal Processes. John Wiley & Sons, Inc., Hoboken, NJ, USA. https://doi.org/10.1002/9781118671603

[21] Park, J., Kim, T., Leigh, S.B. (2014). Application of a phase-change material to improve the electrical performance of vertical-building-added photovoltaics considering the annual weather conditions. Solar Energy, 105: 561-574. https://doi.org/10.1016/j.solener.2014.04.020

NOMENCLATURE

C	specific heat, $J \cdot kg^{-1} \cdot K^{-1}$
g	gravitational acceleration, $m \cdot s^{-2}$
H_L	heat of fusion, $kJ \cdot kg^{-1}$
s	thickness, mm
T	temperature, K
T_l	Melting Temperature, K
T_s	Freezing Temperature, K

Greek Symbols

α	absorptivity
β	thermal expansion coefficient, K^{-1}
β_l	liquid fraction
γ	diffuse reflection coefficient
ε	emissivity
ε_p	porosity
η	efficiency
λ	thermal conductivity, $Wm^{-1}\cdot K^{-1}$
μ	dynamic viscosity, $kg\cdot m^{-1}\cdot s^{-1}$
ρ	density, $kg\cdot m^{-3}$
τ	transmissivity

Subscripts

el	electrical
f	heat transfer fluid
g	glass
mf	metal foam
pcm	phase change material
th	thermal